

Original Article**QSAR studies of histone deacetylase (HDAC) inhibitors by CoMFA, CoMSIA, and molecular docking**

Lei Zhang, Hao Fang, Huawei Zhu, Qiang Wang, Wenfang Xu*

Department of Medicinal Chemistry, School of Pharmacy, Shandong University, Ji'nan, Shandong, China.

ABSTRACT: In order to develop highly potent antitumor agents, three-dimensional quantitative structure-activity relationship (3-D QSAR) studies were conducted using a series of thienyl-based hydroxamic acids. Comparative molecular field analysis (CoMFA) and comparative molecular similarity indices analysis (CoMSIA) methods were applied to provide the structural information for further chemical modification and optimization. ClogP was applied as an additional descriptor in the CoMFA analysis to study the effects of lipophilic parameters on the activity of these compounds, and it did improve the statistical significance of the model. Two molecules were designed based on the 3-D QSAR analysis, their activity values were predicted by the generated model, and their binding mode was elucidated by a docking approach compared to molecules in the dataset.

Keywords: HDAC, QSAR, CoMFA, CoMSIA, docking

1. Introduction

Histone deacetylases (HDACs) are considered to be one of the most interesting and promising targets for the treatment of cancer. More and more scientists pay close attention to them for their intensive correlation with the pathogenesis of cancer. So far, at least 18 HDAC subtypes exist as subdivided into four classes: class I proteins (HDACs 1, 2, 3, and 8), are homologous to the yeast Rpd3 deacetylase; class II enzymes (HDACs 4, 5, 6, 7, 9, and 10), are related to the yeast Hda1 deacetylase; class III (Sirtuins 1-7) are yeast Sir2 homologs, and class IV (HDAC11) has homology to both class I and class II enzymes. It needs to be noted that class I, II, and IV HDACs are all zinc-dependent

hydrolases (1-3).

It is widely believed that alterations in the balance between histone deacetylases (HDACs) and histone acetylase (HATs) play an important role in tumorigenesis. Histone deacetylases and histone acetylase are enzymes responsible for deacetylating and acetylating the amino-terminal tails of histones, respectively. These chromatin changes help regulate transcription and many other nuclear events. Non-histone proteins (such as oncosuppressor p53) and a few cytoplasmic proteins are also accommodated by HDACs/HATs (4). Studies on the molecular pathogenesis of acute myeloid leukemias have shown that the aberrant recruitment of HDACs has a significant role in leukemogenesis. Leukemia-associated fusion proteins (such as promyelocytic leukemia-retinoic acid receptor and acute myeloid leukemia 1 -ETO) recruit HDACs to repress the transcription of genes involved in differentiation and impair the function of p53 (5). HDACs can decrease the half-life of several substrates by exposing the lysine residue for ubiquitylation, and also affect protein location, DNA binding, protein-protein interactions (such as the association of the mainly nuclear DNA-damage-response protein Ku70 with the pro-apoptotic protein BAX) (6-9).

Histone deacetylase inhibitors (HDACi) exert cell-type-specific effects including apoptosis, cell-cycle arrest and differentiation. In leukemias, HDACi include the expression of members of the tumor-necrosis factor-related apoptosis-inducing ligand and FAS death receptor pathways. This induction is responsible for the pro-apoptotic efforts of HDACi (10-13). So far several kinds of HDACi have been studied in clinical trials, and a case in point is that suberoyl anilide hydroxamic acid (SAHA) was approved by the FDA for once-daily oral treatment of advanced cutaneous T-cell lymphoma (CTCL) in 2006.

HDACi can be subdivided into 5 structural categories: short chain fatty acids (such as butyrate and phenylbutyrate) (14-17), hydroxamic acids (such as trichostatin A and SAHA) (18-24), epoxyketone-containing cyclic tetrapeptides (such as trapoxin B and HC-toxin) (25,26), epoxyketone-containing cyclic tetrapeptides (such as CHAP53, apicidin) (27-30), and

*Address correspondence to:

Dr. Wenfang Xu, Department of Medicinal Chemistry, School of Pharmacy, Shandong University, No. 44, West Culture Road, Ji'nan 250012, Shandong, China.
e-mail: xuwenf@sdu.edu.cn

amides (such as MS-275) (Figure 1) (31).

The hydroxamic acids have three structural motifs, including a zinc binding group (ZBG), a linker and an external motif, the so-called "surface recognition motif" (Figure 2) (32).

To obtain more potent HDACis as anti-proliferative agents, Price and coworkers synthesized a series of thienyl-based hydroxamic acids which have excellent potency in the HDAC assay (33). To rationalize the observed variance in inhibitory activity, to propose a possible mechanism of antitumor activity and to guide the synthesis of additional compounds, comparative molecular field analysis (CoMFA) and comparative molecular similarity indices analysis (CoMSIA) were employed to derive three-dimensional quantitative structure-activity relationship (3-D QSAR) models. CoMFA and CoMSIA methods have been the most powerful tools in the 3-D QSAR approach and are used in understanding the mechanism of interactions between various receptors and ligands. Based on the information derived by 3-D QSAR study, two molecules were designed, and their pIC_{50} values were predicted by the generated models.

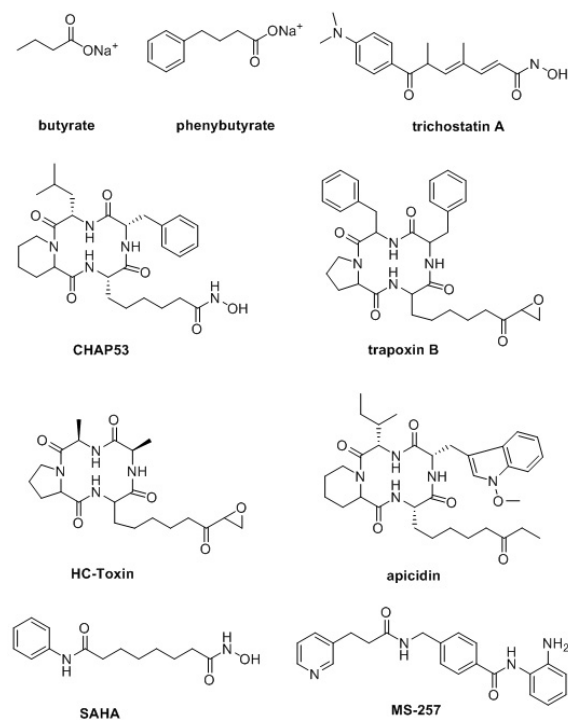


Figure 1. Structure of HDACi molecules from different categories.

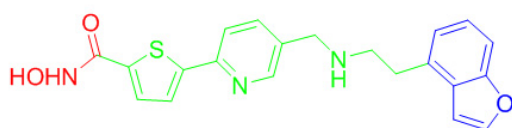


Figure 2. The general structure of hydroxamic acid HDACi. The red part is ZBG, the green part is linker, and the blue part is the surface recognition motif.

As 3-D QSAR is only a ligand based approach, a docking method was used to validate the results. The compounds in the dataset were tested against nuclear extracts which contain a mixture of HDACs, so it is unclear which subtype plays a predominant role, and moreover, only the crystal structure of human HDAC8 is available at the moment. Therefore the *holo*-form crystal structure of HDAC8 (34) was used to study the binding mode of molecules in the dataset and the designed molecules.

2. Materials and Methods

2.1. Data set

Thirty-five molecules selected for the present study were taken from the published work of Price and coworkers (33). The structure and activity data of the compounds belonging to various chemical classes are given in Table 1. The 3-D QSAR models were generated using a training set of 28 molecules. The predictive ability of the resulting models was evaluated using a test set of 7 molecules.

2.2. Molecular modeling

The docking studies were performed using Sybyl 7.0 (Tripos Inc., St. Louis, MO, USA) software running on a DELL Precision 390 workstation and the remaining computational studies were performed using the Sybyl 7.3 (Tripos Inc.) program running on a DELL Precision 360 workstation. The molecular structures were built based on the bioactive conformation of compound **5u** which was generated by a docking procedure. Energy minimization was performed using Powell optimization in the presence of the Tripos force field with a convergence criterion of 0.05 kcal/mol·Å and then assigned with the Gasteiger-Hückel charges.

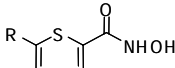
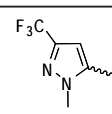
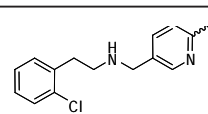
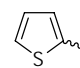
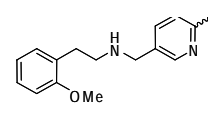
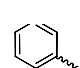
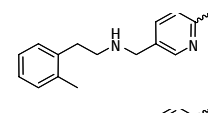
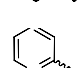
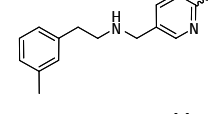
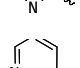
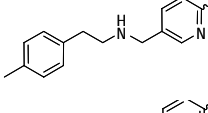
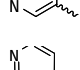
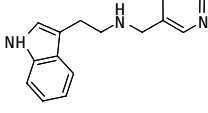
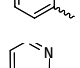
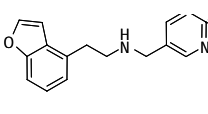
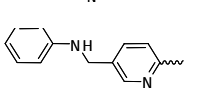
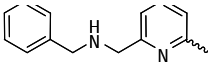
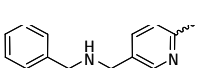
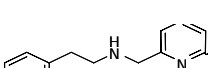
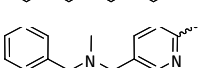

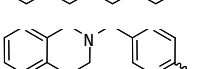
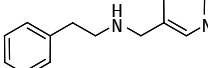
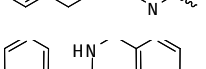
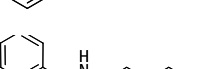
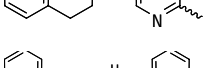
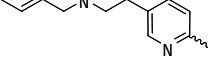
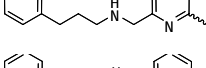
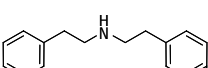
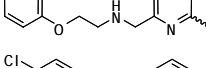

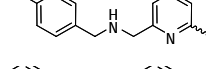
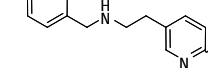
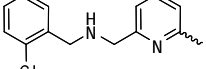
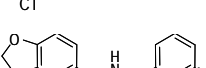
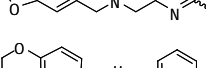
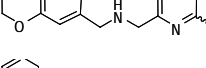
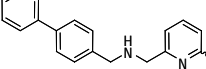
2.3. Alignment rules

There are several molecular alignment rules, such as atom based, structure based, docking based, field based, pharmacophore based approaches and so on. Wang and Zhu in our lab have reported the application of the above methods (35,36). Herein molecular superimposition was carried out by using the relatively simple atom fit method, and a favorable alignment was derived. The reference structure for RMSD fitting was shown in Figure 3.

2.4. CoMFA and CoMSIA analysis

CoMFA steric and electrostatic fields were separately calculated using the sp^3 carbon probe atom with a *van der Waals* radius of 2.0 Å and +1 charge. The energies were truncated to ± 30 kcal/mol, and the electrostatic

Table 1. Structures and bioactivity data of the compounds in the data set

					
Compounds	R	HDACa (IC ₅₀ , μM)	Compounds	R	HDACa (IC ₅₀ , μM)
ADS10038		0.750	5o		0.006
3a		2.500	5p		0.017
3b		0.900	5q		0.008
3c		0.243	5r		0.009
3d		1.130	5s		0.014
*3e		1.260	5t		0.008
3f		0.186	5u		0.004
5a		0.016	7a		0.359
5b		0.016	7b		0.581
5c		0.035	*9		0.080
*5d		0.030	13a		0.009
5e		0.012	13b		0.031
5f		0.018	13c		0.013
5g		0.011	*13d		0.009
5h		0.009	#z1		-
*5i		0.007	#z2		-
5j		0.008			
5k		0.011			
5l		0.007			
5m		0.009			
*5n		0.012			

* Molecules in test set; # molecules designed. The data are referring to Price *et al.*, Bioorg Med Chem Lett. 2007; 17:363-369.

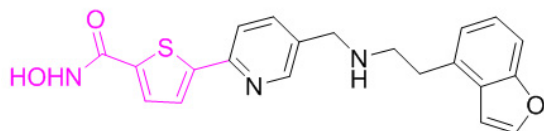


Figure 3. Structure of the reference molecule 5u. The magenta part was used for atomic alignment.

contributions were ignored at the lattice intersection with maximal steric interactions. The CoMFA fields generated were automatically scaled by the CoMFA-STD method.

The CoMSIA method involves a common probe atom and similarity indices calculated at regularly spaced grid intervals. The same grid constructed for the CoMFA fields was used for the CoMSIA calculation. CoMSIA can derive hydrophobic, H-bond donor and acceptor fields in addition to CoMFA steric and electrostatic fields. The distance dependence between the grid point and each atom was determined by Gaussian function through the similarity indices calculated at all grid points, and a default value of 0.3 was used as an attenuation factor.

2.5. Partial least square (PLS) analysis

The predictive values of models were evaluated by leave-one-out (LOO) cross validation method, and an optimal number of components obtained from each calculation were used to generate the final model without cross validation. The result from a cross validation analysis was depicted as r^2_{cv} which is defined as

$$r^2_{cv} = 1 - \text{PRESS} / \sum(Y - Y_{\text{mean}})^2$$

where

$$\text{PRESS} = \sum(Y - Y_{\text{pred}})^2$$

2.6. Test set validation

It is widely considered that more than 0.5 of $q^2(r^2_{cv})$ value is a necessary condition for a predictive QSAR model. Many methods are established to validate the predictive ability of the generated model, such as Tropsha's validation criteria (37,38). We used a relatively simple method to investigate the robustness of the models derived by CoMFA and CoMSIA methods. The linear correlation coefficient R^2 between the bioactivity and the predicted activity of the test set molecules was used to evaluate the predictive ability of the derived model.

2.7. Docking analysis

The crystal structure of HDAC8 was obtained from the protein data bank (PDB entry: 1t64 (1.90Å)). Compound **5u** and the design molecules were docked to the active site of HDAC8. Since there was no water in the active site, before docking, all water molecules were removed from the crystal structure, hydrogen

atoms were added, and Amber charge was loaded. The docking studies were performed using the FlexX module in Sybyl 7.0, and the maximum number of poses per ligand was set to 90. One of the symmetrical subunits formed by chain A was selected as the protein for the docking study to save computational time. Cscore was applied to evaluate the docking results. The active site was defined as 6.5Å radius circles around the ligand TSN386 (trichostatin A) and other parameters were set as default.

3. Results and Discussion

3.1. CoMFA

A good alignment of the dataset is essential for a predictive 3D-QSAR model. The docking method was first applied to align all the molecules, but too many flexible bonds made it difficult to align the molecules in the dataset to the same position. Therefore only the structure of the most bioactive compound **5u** was derived by docking, the rest of the molecules were constructed using **5u** as a reference, then the alignment was carried out by atomic fit (Figure 4).

Table 2 summarizes the PLS results of the CoMFA and CoMSIA analysis. It is obvious that application

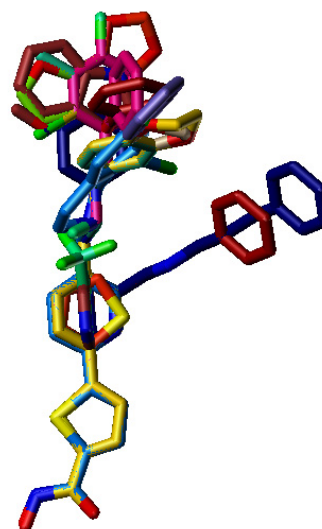


Figure 4. Alignment of the molecules in the data set.

Table 2. Summary of PLS results

Parameters	CoMFA	CoMFA (ClogP)	CoMSIA
r^2_{cv}	0.848	0.850	0.917
ONC	2	6	8
r^2	0.922	0.985	0.991
SEE	0.232	0.110	0.090
F	147.482	234.360	262.346
Steric	0.691	0.558	0.190
Electrostatic	0.309	0.347	-
Hydrophobic	-	-	0.580
Donor	-	-	0.231
ClogP	-	0.068	-

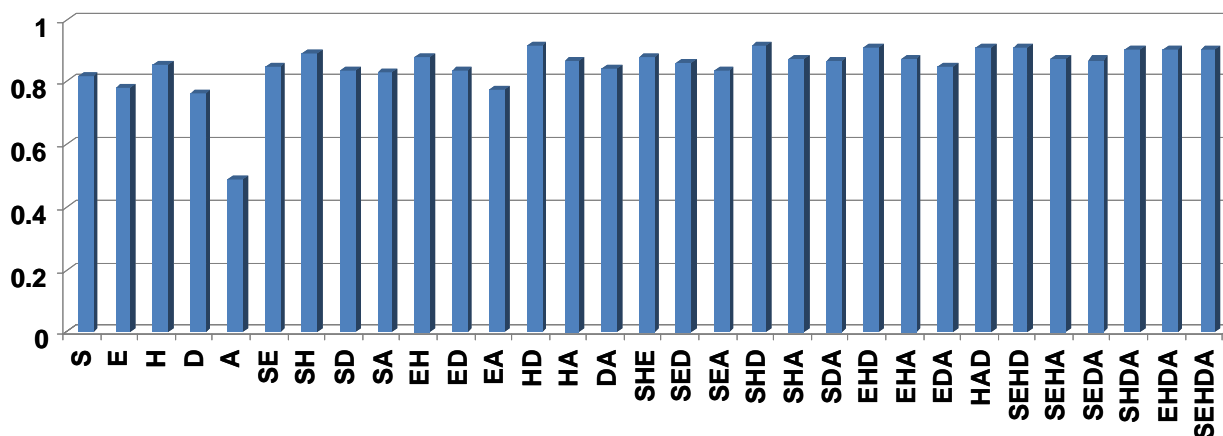


Figure 5. Results of all the possible CoMSIA field combinations. S, steric; E, electrostatic; H, hydrophobic; D, H-bond donor; A, H-bond acceptor.

of ClogP improved the statistical significance of the CoMFA model. All the statistical parameters showed that the model derived considering ClogP is more robust. Therefore we can conclude that the hydrophobic property of the molecules plays an important role in their activity.

3.2. CoMSIA

CoMSIA analysis was performed using steric, electrostatic, hydrophobic, H-bond donor and acceptor descriptors. The five different fields can form various combinations to study the role of each field. Herein r^2_{cv} values of the 31 combinations were derived by using the SAMPLS method (Figure 5). Among these combinations hydrophobic field has the highest r^2_{cv} in the single field analysis ($r^2_{cv} = 0.851$), steric has the second rank ($r^2_{cv} = 0.819$). The combination of hydrophobic and H-bond donor has the highest r^2_{cv} value in the two field analysis (0.912). The addition of the steric field ascended the r^2_{cv} value to 0.916 which is the highest r^2_{cv} in these combinations. Therefore, steric, hydrophobic and H-bond donor fields were used to generate the final CoMSIA model.

As shown in Table 3, the CoMSIA model is more statistically significant than the two CoMFA models.

3.3. Validation of 3-D QSAR models

The significance and utility of 3-D QSAR models was validated by predicting the activity of test molecules which were not included in model development. Compounds **3e**, **5d**, **5i**, **5n**, **5s**, **9**, and **13d** were selected as a test set to verify the robust and predictive ability of the derived models. The CoMFA model generated considering ClogP in addition to electrostatic and steric fields has a higher R^2 (Figure 6). It is also evidence that the hydrophobic property of the molecules is essential for their enzyme inhibitory activity. The CoMSIA model is the most statistically significant for the

Table 3. Actual activity, ClogP and predicted activity of the data set

Compounds	pIC ₅₀	ClogP	CoMFA	CoMFA (ClogP)	CoMSIA
13a	8.05	2.527	7.841	7.943	7.931
13b	7.51	2.446	7.746	7.623	7.556
13c	7.89	2.670	7.844	7.955	7.944
*13d	8.05	2.492	7.826	7.953	7.902
3a	5.60	2.178	6.177	5.638	5.680
3b	6.05	2.310	6.320	6.096	5.893
3c	6.61	1.062	6.508	6.644	6.585
3d	6.89	0.852	6.469	6.800	6.910
*3e	5.90	0.852	6.209	6.266	6.704
3f	6.73	0.111	6.372	6.672	6.963
5a	7.80	2.009	7.532	7.821	7.835
5b	7.80	1.588	7.898	7.857	7.862
5c	7.46	2.664	7.879	7.507	7.486
*5d	7.52	2.949	7.754	7.300	7.266
5e	7.92	2.527	7.995	8.095	7.991
5f	7.74	2.906	7.818	7.586	7.704
5g	7.96	2.395	7.900	8.036	7.933
5h	8.05	2.301	7.961	7.915	8.020
*5i	8.15	2.301	7.893	7.721	7.873
5j	8.10	1.553	8.071	8.030	7.974
5k	7.96	1.512	8.104	7.971	7.929
5l	8.15	3.476	8.134	8.260	8.206
5m	8.05	2.670	7.999	8.017	8.004
*5n	7.92	2.670	7.911	7.923	8.102
5o	8.22	3.240	8.020	7.951	8.343
5p	7.77	2.446	8.031	7.846	7.822
5q	8.10	2.976	8.130	8.163	8.188
5r	8.05	3.026	8.027	7.994	8.064
*5s	7.85	3.026	8.007	8.002	8.022
5t	8.10	2.517	8.071	8.133	8.065
5u	8.40	3.087	8.169	8.319	8.209
7a	6.44	1.588	6.312	6.397	6.447
7b	6.24	2.906	6.146	6.198	6.242
*9	7.10	3.645	7.720	7.291	7.609
ADS	6.12	1.688	6.284	6.202	6.172

* Molecules in test set.

training set itself, but to the test set, its predictive ability is the poorest. This is because the CoMSIA method is more sensitive to the structural diversity, and the alignment of the dataset is not perfect. Table 3 shows details of predictive properties of the three models.

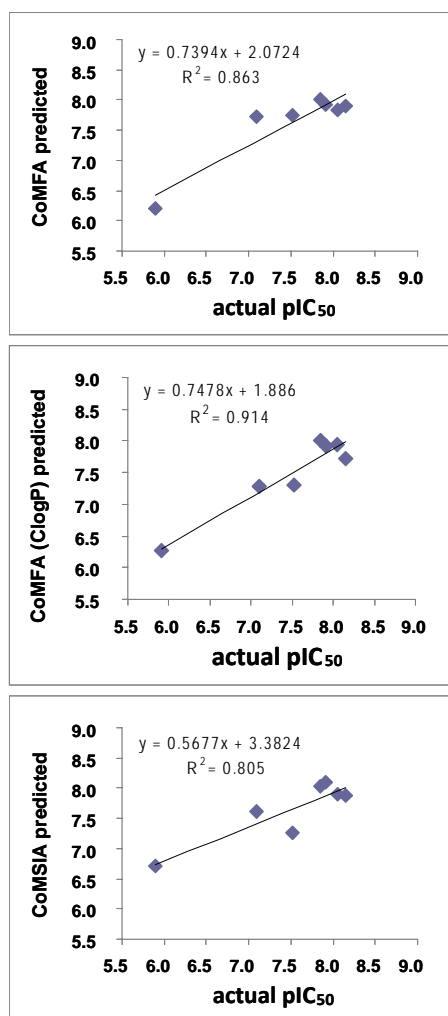


Figure 6. Scatterplot of actual pIC_{50} versus predicted pIC_{50} of the test set molecules.

3.4. 3-D QSAR contour maps

CoMFA and CoMSIA contour maps were generated to visualize the field distribution of the 3-D QSAR models. Figure 7a shows the steric contour maps around molecule **5u**. The evidence that the high steric tolerance region (the big green contour) is located at the position of the externa motif indicates that the larger substituent herein is essential for high activity. For example, the aromatic ring of molecule **5o**, **5t**, and **5u** is very bulky in this region, and all of them have high enzyme inhibiting activity (pIC_{50} = 8.22, 8.10, and 8.40, respectively). Compounds in class 3 are less active than those in other classes (mean pIC_{50} = 6.14), because their corresponding parts are too small to fit in this region (Figure 7b). Because the phenyl rings of compound **7a** and **7b** stretch to somewhere else (Figure 7c) is a reason for their low activity (pIC_{50} = 6.44, 6.24). The blue contours in Figure 7a describe a region where a positive charged group enhances activity. The big blue region is around the $-NH_2$ - group in the linker suggesting that increasing positive charges in this area can improve activity. Most molecules have this feature but because molecules in

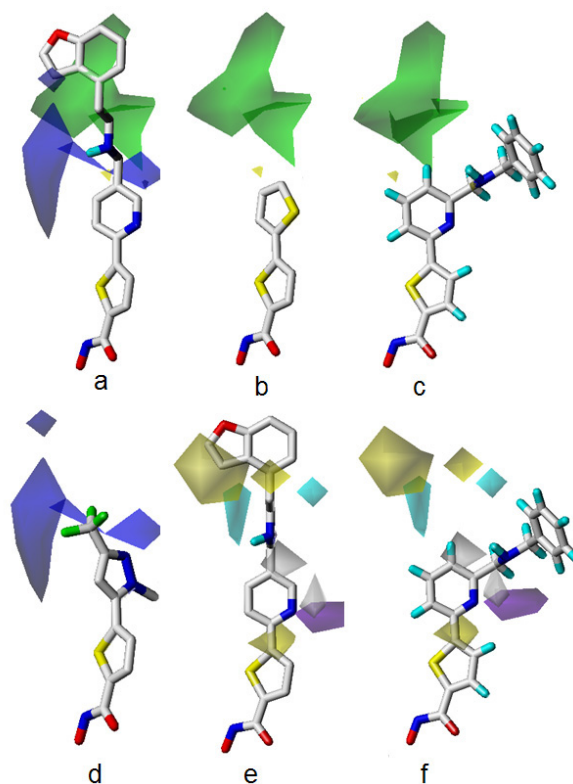


Figure 7. Contour maps of the QSAR analysis. a, CoMFA steric fields and electrostatic fields around **5u**; b and c, CoMFA steric fields around **3a** and **7a**; d, electrostatic fields around **ADS** (color code: steric favored, green; positive charge favored, blue); e and f, CoMSIA hydrophobic and H-bond donor fields around **5u** and **7a** (color code: hydrophobic favored, yellow; hydrophobic disfavored, white; H-bond donor favored, cyan; H-bond donor disfavored, purple).

class 3 cannot reach into this region it is believed to be another cause of their low activity, one negative charge taking the fluorine atom of **ADS** also is considered to be an important reason for its low activity (Figure 7d). The steric fields of CoMSIA provide similar information as CoMFA, so they will not be described in detail here. CoMSIA hydrophobic field has the most contribution to the model, it is further evidence that the hydrophobic properties of the molecules plays an important role in the activity. In the hydrophobic contour plots (Figure 7e), the favorable yellow bulk overlapping the aromatic ring means improving the hydrophobic property of this part is essential for high enzyme inhibiting activity. The unfavorable white regions located around the $-NH$ -group in the linker indicates hydrophilicity is required in this region. The H-bond donor favorable contours (cyan) located at the hydrogen atom region of the $-NH_2$ - group indicates that increasing H-bond donors in this part will improve inhibitory activity. Lack of occupation of the hydrophobic region (the phenyl ring) and the adjacent H-bond donor unfavorable purple region (the $-NH_2$ -group) are other reasons for the low activity of **7a** and **7b** (Figure 7f).

Two carbamido groups containing hydroxamic acids were designed based on the information given by the above analysis. Their predicted pIC_{50} values are 6.916 and 7.217, respectively.

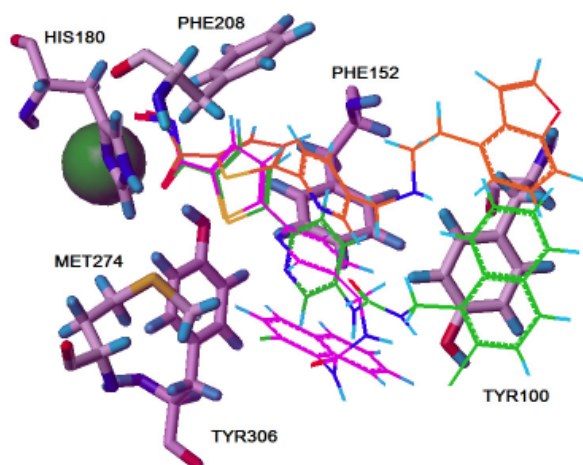


Figure 8. Docking of the designed molecules **z1**, **z2**, and the most potent compound **5u** into the active site of HDAC8. The orange molecule is **5u**, the green one is **z1**, and the magenta one is **z2**. The green ball is zinc.

3.5. Docking analysis

The predictive activities of the designed molecules are not as high as expected. Therefore molecular docking was used to further clarify the binding mode of the molecules and to determine whether it is necessary to synthesize the designed molecules.

The crystal structure of HDAC8 reveals a channel formed by several residues, the core residues are labeled in Figure 8 (TYR100, PHE152, HIS180, PHE208, MET274, and TYR306). In the end of the channel, there is a zinc ion for binding with the hydroxamic acid part (bidentate chelation). A significant π - π stacking interaction can be found in the aromatic ring of the external motif of **z1** and **5u** with the phenyl ring of TYR100. The linker locating the channel has hydrophobic and π - π stacking interactions with the amino acids forming a hydrophobic pocket. The -NH-group in the linker of **z1** and **z2** has H-bond interactions with the hydroxyl group of TYR100. This suggests that a strong chelating interaction could stabilize the compound in the active site, and that hydrophobic and H-bond binding would also enhance the interaction between the molecule and the protein.

The total docking scores of **5u**, **z1**, and **z2** are -31.532, -39.420, and -41.461, respectively. The binding modes and the docking scores both emphasize the necessity of the synthesis of the two designed compounds, and their synthetic work is under way.

4. Conclusions

Two 3-D QSAR methods, CoMFA and CoMSIA, were applied to a series of thienyl-based hydroxamic acids as HDAC inhibitors. ClogP was considered in the CoMFA study, and it improved the robustness and predictive ability of the generated model. To study the effect of the five fields in CoMSIA, r^2_{cv} values of 31 combinations

were derived using the SAMPLS method. The steric, hydrophobic and H-bond donor fields proved to be the most important. The contour maps of both methods explained the influence of substitutions on HDACs activity. Two molecules were designed based on the above models, and their activities were predicted. Although the predicted activities are not very high, the binding mode clarified by a docking approach showed they are worth synthesizing. Their bioactivities will also be a validation of the generated model.

Acknowledgments

This work was supported by National Nature Science Foundation of China (Grant Nos. 30772654 and 36072541) and the Ph.D. Programs Foundation of Ministry of Education of PR China (No. 20060422029) and National High Technology Research and Development Program of China (863 project; Grant No. 2007AA02Z314).

References

1. Minucci S, Pelicci PG. Histone deacetylase inhibitors and the promise of epigenetic (and more) treatments for cancer. *Nat Rev Cancer*. 2006; 6:38-51.
2. Vannini A, Volpari C, Filocamo G, Casavola EC, Brunetti M, Renzoni D, Chakravarty P, Paolini C, Francesco RD, Gallinari P, Steinkühler C, Marco SD. Crystal structure of a eukaryotic zinc-dependent histone deacetylase, human HDAC8, complexed with a hydroxamic acid inhibitor. *Proc Natl Acad Sci U S A*. 2004; 101:15064-15069.
3. Blander G, Guarente L. The SIR2 family of protein deacetylases. *Annu Rev Biochem*. 2004; 73:417-435.
4. Bode AM, Dong ZG. Post-translational modification of p53 in tumorigenesis. *Nat Rev Cancer*. 2004; 4:793-805.
5. Minucci S, Nervi C, Lo Coco F, Pelicci PG. Histone deacetylases: a common molecular target for differentiation treatment of acute myeloid leukemias? *Oncogene*. 2001; 20:3110-3115.
6. Giandomenico V, Simonsson M, Grönroos E, Ericsson J. Coactivator-dependent acetylation stabilizes members of the SREBP family of transcription factors. *Mol Cell Biol*. 2003; 23:2587-2599.
7. Grönroos E, Hellman U, Heldin CH, Ericsson J. Control of smad7 stability by competition between acetylation and ubiquitination. *Mol Cell*. 2002; 10:483-493.
8. Jin YH, Jeon EJ, Li QL, Lee YH, Choi JK, Kim WJ, Lee KY, Bae SC. Transforming growth factor- β stimulates p300-dependent RUNX3 acetylation, which inhibits ubiquitination-mediated degradation. *J Biol Chem*. 2004; 279:29409-29417.
9. Rausa FM, Hughes DE, Costa RH. Stability of the hepatocyte nuclear factor 6 transcription factor requires acetylation by the CREB-binding protein coactivator. *J Biol Chem*. 2004; 279:43070-43076.
10. Johnstone RW. Histone-deacetylase inhibitors: novel drugs for the treatment of cancer. *Nat Rev Drug Discov*. 2002; 1:287-299.
11. Marks PA, Rifkind RA, Richon VM, Breslow R, Miller T, Kelly WK. Histone deacetylases and cancer: causes and therapies. *Nat Rev Cancer*. 2001; 1:194-202.

12. Insinga A, Monestiroli S, Ronzoni S, Gelmetti V, Marchesi F, Viale A, Altucci L, Nervi C, Minucci S, Pelicci PG. Inhibitors of histone deacetylases induce tumor-selective apoptosis through activation of the death receptor pathway. *Nature Med.* 2005; 11:71-76.
13. Nebbioso A, Clarke N, Voltz E, Germain E, Ambrosiino C, Bontempo P, Alvarez R, Schiavone EM, Ferrara F, Bresciani F, Weisz A, Lera ARD, Gronemeyer H, Altucci L. Tumor-selective action of HDAC inhibitors involves TRAIL induction in acute myeloid leukemia cells. *Nature Med.* 2005; 11:77-84.
14. Krämer OH, Göttlicher M, Heinzel T. Histone deacetylase as a therapeutic target. *Trends Endocrin Meta.* 2001; 12:294-300.
15. Archer SY, Meng SF, Shei A, Hodin RA. p21WAF1 is required for butyrate-mediated growth inhibition of human colon cancer cells. *Proc Natl Acad Sci U S A.* 1998; 95:6791-6796.
16. Demary K, Wong L, Spanjaard RA. Effects of retinoic acid and sodium butyrate on gene expression, histone acetylation and inhibition of proliferation of melanoma cells. *Cancer Lett.* 2001; 163:103-108.
17. Phiel CJ, Zhang F, Huang EY, Guenther MG, Lazar MA, Klein PS. Histone deacetylase is a direct target of valproic acid, a potent anticonvulsant, mood stabilizer, and teratogen. *J Biol Chem.* 2001; 276:36734-36741.
18. Woo SH, Frechette S, Khalil EA, Bouchain G, Vaisburg A, Bernstein N, Moradei O, Leit S, Allan M, Fournel M, Trachy-Bourget M, Li Z, Besterman JM, Delorme D. Structurally simple trichostatin A-like straight chain hydroxamates as potent histone deacetylase inhibitors. *J Med Chem.* 2002; 45:2877-2885.
19. Remiszewski SW, Sambucetti LC, Atadja P, Bair KW, Cornell WD, Green MA, Howell KL, Jung M, Kwon P, Trogani N, Walker H. Inhibitors of human histone deacetylase: synthesis and enzyme and cellular activity of straight chain hydroxamates. *J Med Chem.* 2002; 45:753-757.
20. Massa S, Mai A, Sbardella G, Esposito M, Ragno R, Loidl P, Brosch G. 3-(4-Aroyl-1H-pyrrol-2-yl)-N-hydroxy-2-propenamides, a new class of synthetic histone deacetylase inhibitors. *J Med Chem.* 2001; 44:2069-2072.
21. Mai A, Massa S, Ragno R, Esposito M, Sbardella G, Nocca G, Scatena R, Jesacher F, Loidl P, Brosch G. Binding mode analysis of 3-(4-Benzoyl-1-methyl-1H-2-pyrrolyl)-N-hydroxy-2-propenamide: a new synthetic histone deacetylase inhibitor inducing histone hyperacetylation, growth inhibition, and terminal cell differentiation. *J Med Chem.* 2002; 45:1778-1784.
22. Mai A, Massa S, Ragno R, Cerbara L, Jesacher F, Loidl P, Brosch G. 3-(4-Aroyl-1-methyl-1H-2-pyrrolyl)-N-hydroxy-2-alkylamides as a new class of synthetic histone deacetylase inhibitors. 1. Design, synthesis, biological evaluation, and binding mode studies performed through three different docking procedures. *J Med Chem.* 2003; 46:512-524.
23. Jung M, Brosch G, Kolle D, Scherf H, Gerhauer C, Loidl P. Amide analogues of trichostatin A as inhibitors of histone deacetylase and inducers of terminal cell differentiation. *J Med Chem.* 1999; 42:4669-4679.
24. Butler LM, Agus DB, Scher HI, Higgins B, Rose A, Cordon-Cardo C, Thaler HT, Rifkind RA, Marks PA, Richon VM. Suberoylanilide hydroxamic acid, an inhibitor of histone deacetylase, suppresses the growth of prostate cancer cells *in vitro* and *in vivo*. *Cancer Res.* 2000; 60:5165-5170.
25. Itazaki H, Nagasshima K, Sugita K, Yoshida H, Kawamura Y, Yasuda Y, Matsumoto K, Ishii K, Uotani N, Nakai H, Terui A, Yoshimatsu S, Ikenishi Y, Nakagawa Y. Solation and structural elucidation of new cyclotetrapeptides, trapoxins A and B, having detransformation activities as antitumor agents. *J Antibiot Tokyo.* 1990; 43:1524-1532.
26. Brosch G, Ransom R, Lechner T. Inhibition of maize histone deacetylases by HC toxin, the host-selective toxin of *cochliobolus carbonum*. *Plant Cell.* 1995; 7:1941-1950.
27. Darkin-Rattray SJ, Gurnett AM, Myers RW, Dulski PM, Crumley TM, Allocco JJ, Cannova C, Meinke PT, Colletti SL, Bedmarek MA, Singh SB, Goetz MA, Dombrowski AW, Polishook JD, Schmatz DM. Apicidin: a novel antiprotozoal agent that inhibits parasite histone deacetylase. *Proc Natl Acad Sci U S A.* 1996; 93:13143-13147.
28. Furumai R, Komatsu Y, Nishino N, Khochbin S, Yoshida M, Horinouchi S. Potent histone deacetylase inhibitors built from trichostatin A and cyclic tetrapeptide antibiotics including trapoxin. *Proc Natl Acad Sci U S A.* 2001; 98:87-92.
29. Li KW, Wu J, Xing W, Simon JA. Total synthesis of the antitumor depsipeptide FR-901228. *J Am Chem Soc.* 1996; 118:7237-7238.
30. Nakajima H, Kim YB, Terano H, Yoshida M, Horinouchi S. FR901228, a potent antitumor antibiotic, is a novel histone deacetylase inhibitor. *Exp Cell Res.* 1998; 241:126-133.
31. Saito A, Yamashita T, Mariko Y, Nosaka Y, Tsuchiya K, Ando T, Suzuki T, Tsuruo T, Nakanishi O. A synthetic inhibitor of histone deacetylase, MS-27-275, with marked *in vivo* antitumor activity against human tumors. *Proc Natl Acad Sci U S A.* 1999; 96:4592-4597.
32. Paris M, Porcelloni M, Binaschi M, Fattori D. Histone deacetylase inhibitors: from bench to clinic. *J Med Chem.* 2008; 51:1505-1529.
33. Price S, Bordogma W, Braganza R, *et al.* Identification and optimisation of a series of substituted 5-pyridin-2-yl-thiophene-2-hydroxamic acids as potent histone deacetylase (HDAC) inhibitors. *Bioorg Med Chem Lett.* 2007; 17:363-369.
34. Somoza JR, Skene RJ, Katz BA, *et al.* Structural snapshots of human HDAC8 provide insights into the class I histone deacetylases. *Structure.* 2004; 12:1325-1334.
35. Wang Q, Chen MY, Zhu HW, Zhang J, Fang H, Wang BH, Xu WF. Design, synthesis, and QSAR studies of novel lysine derives as amino-peptidase N/CD13 inhibitors. *Bioorg Med Chem.* 2008; 16:5473-5481.
36. Zhu HW, Fang H, Wang LY, Hu WX, Xu WF. 3D-QSAR study with pharmacophore-based molecular alignment of hydroxamic acid-related phosphinates that are aminopeptidase N inhibitors. *Drug Discov Ther.* 2008; 2:52-57.
37. Golbraikh A, Tropsha A. Beware of q2! *J Mol Graph Model.* 2002; 20:269-276.
38. Golbraikh A, Shen M, Xiao Z, Xiao YD, Lee KH, Tropsha A. Rational selection of training and test sets for the development of validated QSAR models. *J Comput Aided Mol Des.* 2003; 17:241-253.

(Received April 14, 2009; Accepted April 23, 2009)